Speed of a swimming sheet in Newtonian and viscoelastic fluids

Moumita Dasgupta,[1] Bin Liu,[2] Henry C. Fu,[2,3] Michael Berhanu,[1,4] Kenneth S. Breuer,[2]
Thomas R. Powers,[2,5] and Arshad Kudrolli[1]

[1]*Department of Physics, Clark University, Worcester, Massachusetts 01610, USA*
[2]*School of Engineering, Brown University, Providence, Rhode Island 02912, USA*
[3]*Mechanical Engineering Department, University of Nevada, Reno, Reno, Nevada 89509, USA*
[4]*Matière et Systèmes Complexes (MSC), Université Paris Diderot, CNRS (UMR 7057), 75013 Paris, France*
[5]*Department of Physics, Brown University, Providence, Rhode Island 02912, USA*

(Received 2 October 2012; published 17 January 2013)

We measure the swimming speed of a cylindrical version of Taylor's swimming sheet in viscoelastic fluids, and find that depending on the rheology, the speed can either increase or decrease relative to the speed in a Newtonian viscous fluid. The swimming stroke of the sheet is a prescribed propagating wave that travels along the sheet in the azimuthal direction. The measurements are performed with the sheet immersed in a fluid inside a cylindrical tank under torque-free conditions. Swimming speeds in the Newtonian case are found to be consistent with calculations using the Stokes equation. A faster swimming speed is found in a viscoelastic fluid that has a viscosity independent of shear rate. By contrast, a slower swimming speed is found with more complex shear-thinning viscoelastic fluids which have multiple relaxation time scales as well. These results are compared with calculations with Oldroyd-B fluids which find a decreasing swimming speed with Deborah number given by the product of the fluid elastic relaxation time scale and the driving frequency.

DOI: 10.1103/PhysRevE.87.013015 PACS number(s): 47.63.Gd, 47.20.Gv, 83.50.Jf

I. INTRODUCTION

Many examples of microorganisms swimming through viscoelastic fluids can be found in nature, including sperm swimming through cervical mucus and *Helicobacter pylori* in gastric mucus [1]. Because of their small size, the Reynolds number is small and inertial effects are negligible. Net swimming translation typically occurs due to a broken symmetry as in a traveling-wave deformation of the sperm flagellum or a chiral or helical motion of some bacteria. Taylor considered the corresponding problem of an infinite planar sheet with a prescribed traveling-wave form [2]. He showed that the swimming speed is proportional to the phase velocity and to the square of the wave amplitude. Extending this work to viscoelastic fluids, Lauga [3] recently calculated the speed of a swimmer in an Oldroyd-B model fluid which has a single relaxation time and a shear-rate-independent viscosity. He found that the ratio $v_{N\text{-}N}/v_N$ of the swimming speed in the non-Newtonian fluid to the swimming speed in a Newtonian fluid decreases with increasing Deborah number De as $v_{N\text{-}N}/v_N = 1/(1+\mathrm{De}^2)$ when the solvent viscosity is small compared to the polymer contribution to the viscosity. Here De is the product of the relaxation time constant of the fluid and the driving frequency. Fu, Powers, and Wolgemuth [4] found a similar relation for small-amplitude waves on an infinitely long filament in a fluid described by the Oldroyd-B model.

Several issues arise in further developing and comparing such calculations with actual swimming speeds of microorganisms. An organism can change form and frequency of stroke in response to changes in the fluid properties, making direct comparisons difficult [5]. Furthermore, biological viscoelastic fluids are far more complex with multiple relaxation time scales and shear-thinning rheology which are highly dependent on concentration and *p*H [6]. Numerical simulations with finite-length sheets in idealized viscoelastic fluids have shown that swimming speeds and efficiency can be enhanced at $\mathrm{De} \approx 1$ for nonsinusoidal large-amplitude undulations, where the amplitude increases from head to tail of the sheet [7]. Enhanced swimming speeds have also been observed with a finite-length model helical flagellum in Boger fluids, with the greatest enhancement observed again near $\mathrm{De} \approx 1$, where the Deborah number is defined as the product of the relaxation rate and the rotation period [8]. Therefore, the agreement between the recent observation [9] of swimming speeds of *Caenorhabditis elegans* in various concentrations of carboxymethyl cellulose (CMC) and the theoretical calculation by Lauga is somewhat surprising because of the significant differences in the geometry and the complexity of the fluids investigated.

In this paper, we introduce an apparatus based on Taylor's swimming sheet to investigate the speed of a swimmer in various non-Newtonian fluids. We first show that the system captures the essence of the idealized Taylor swimming sheet by comparing swimming speed with numerical simulations and analytical calculations using the Stokes equation in the same geometry. We then discuss the swimming speed measured with several kinds of viscoelastic fluids including a viscoelastic Boger fluid which has constant viscosity over a range of shear rates, and more complex shear-thinning viscoelastic fluids. We provide evidence that the ratio of swimming speeds is not always less than 1, and depends on the viscoelastic nature of the fluid.

II. CYLINDRICAL TAYLOR SWIMMER

In order to perform an experiment with a finite-sized swimming sheet, we consider a cylindrical sheet, deformed by traveling bending waves and with an average radius R_1 immersed inside a cylindrical tank with a radius R_2. The cylindrical geometry further simplifies the analysis since there are no complicating effects from free ends. The swimming

speed of this cylindrical Taylor swimmer can be calculated using the Stokes equations and imposing nonslip boundary conditions on the swimmer. Because of the rotary geometry, torque-free conditions are imposed on the swimmer instead of the force-free conditions of the original planar Taylor-sheet swimmer. The stroke of the swimmer is a traveling wave that propagates around the cylindrical sheet. It is simplest to describe the wave in the frame that rotates with the wave. In this frame the peaks and the troughs of the wave are stationary, but the material points of the wave move clockwise, tangentially to the inextensible sheet with speed v. Our wave has two peaks, so the shape of the sheet is given in this frame as

$$\mathbf{R}(\Theta) = (R_1 + b\sin 2\Theta)\,\hat{\mathbf{R}}, \tag{1}$$

where R and Θ are the polar coordinates in the traveling-wave frame. To first order in b/R_1, the arclength s along the sheet is related to the angle Θ by

$$\Theta(s) \approx s/R_1 + \frac{b}{2R_1}\left[\cos\left(\frac{2s}{R_1}\right) - 1\right]. \tag{2}$$

To get the velocity of the material points in the traveling-wave frame, we label the points by their arclength coordinate s_0 at time $t = 0$, which will have an angle $\Theta_{s_0,t} = \Theta(s_0 - vt)$ at time t and position

$$\mathbf{R}(s_0,t) = (R_1 + b\sin 2\Theta_{s_0,t})\hat{\mathbf{R}}(\Theta_{s_0,t}). \tag{3}$$

Differentiating the position $\mathbf{R}(s_0,t)$ with respect to t at fixed s_0 and expressing the result in terms of Θ leads to

$$\mathbf{V}(\Theta,t) = -v\left[\hat{\Theta} + 2\frac{b}{R_1}\hat{\mathbf{R}}\cos 2\Theta\right]. \tag{4}$$

It is simplest to calculate the swimming speed in the the "swimmer frame," the frame that rotates with the material points of the sheet. If the sheet makes one revolution in period T, the swimmer frame rotates at an angular velocity $\Omega_{\text{sheet}} = 2\pi/T$ relative to the traveling-wave frame. For small deformations, the perimeter of the sheet is unchanged from that of a circle of radius R_1 up to first order in b/R_1, so $v = \Omega_{\text{sheet}}R_1$. The traveling-wave frame rotates counterclockwise relative to the swimmer frame, so that the angle θ measured from the x axis of the swimmer frame is related to the angle Θ measured from the x axis of the traveling-wave frame by $\theta = \Theta + vt/R_1 = \Theta + \Omega_{\text{sheet}}t$. Likewise $\hat{\mathbf{R}}(\Theta) = \hat{\mathbf{r}}(\theta)$, and $\hat{\Theta}(\Theta) = \hat{\theta}(\theta)$, and the velocity $\mathbf{v}$ of material points in the swimming frame is related to the velocity of material points in the traveling-wave frame by $\mathbf{v} = \mathbf{V} + \Omega_{\text{sheet}}\hat{\mathbf{z}} \times \mathbf{R}$, or

$$\begin{aligned}\mathbf{v} = &-2\Omega_{\text{sheet}}b\cos\left[2(\theta - \Omega_{\text{sheet}}t)\right]\hat{\mathbf{r}} \\ &+ \Omega_{\text{sheet}}b\sin\left[2(\theta - \Omega_{\text{sheet}}t)\right]\hat{\theta}.\end{aligned} \tag{5}$$

It is interesting to draw a contrast between this expression for the velocity of material points on a curved sheet with small ripples and the corresponding expression used by Taylor for the flat sheet [2]. For the flat sheet with small ripples, the condition of inextensibility leads to horizontal components of the velocity of the wave which are second order in amplitude. These components make a contribution to the swimming velocity that is fourth order, and therefore may be disregarded at leading order [2]. In contrast, the inextensibility of the cylindrical sheet leads to azimuthal components that are *first order* in the amplitude b, and these components must not be disregarded when calculating the leading-order swimming speed.

Imposing the no-slip boundary conditions on the swimmer and the wall and solving the Stokes equations in polar coordinates leads to

$$\Omega^N_{\text{swim}} = g_f\,\Omega_{\text{sheet}}, \tag{6}$$

where g_f is a nondimensional geometric factor which depends on the amplitude of the wave and the size of the tank relative to the size of the swimmer, and is given by

$$g_f = \frac{2b^2}{R_1^2}\frac{3(1 + 6\alpha^2 + \alpha^4)}{4(1 - \alpha^2)^2}, \tag{7}$$

to leading order in b/R_1, and where $\alpha = R_1/R_2$. Thus, the swimming speed has a similar dependence on amplitude and angular phase velocity as in the original Taylor swimming sheet, and the effect of the finite size of the tank is to increase the speed of the swimmer. Such enhancement of swimming has been noted previously as well for a planar sheet swimming near a boundary [10].

In the traveling-wave frame, the geometry of the problem is constant and thus the Stokes problem can be easily solved using COMSOL. In this frame, the material points of the sheet move tangentially to the sheet and so the no-slip boundary condition is a tangential flow at the surface of the deformed sheet. For small deformations, the solutions obtained using COMSOL match the perturbation result for g_f [Eq. (7)] to 1.4%. Using COMSOL, we are also able to investigate large-amplitude deformations and the effects of geometrical asymmetries in the experiments; we describe those results in Sec. IV A in the context of our experimental observations.

Furthermore, for small amplitudes and for small solvent viscosity, the swimming speed in an Oldroyd-B fluid for the cylindrical geometry is

$$\Omega^{N\text{-}N}_{\text{swim}} = \frac{1}{1 + \text{De}^2}\Omega^N_{\text{swim}}, \tag{8}$$

where the superscript N-N denotes swimming speed in a non-Newtonian fluid. In this equation, the Deborah number is defined as

$$\text{De} = \omega\tau, \tag{9}$$

where $\omega = 2\Omega_{\text{sheet}}$ is the oscillation frequency of a material point on the belt. This form is again similar to that for the finite planar Taylor swimming sheet and tells us that for single-relaxation-time viscoelastic fluids, the swimming speed is always lower than that in a Newtonian fluid for the same prescribed traveling wave form.

III. EXPERIMENTAL APPARATUS

A schematic of our experimental apparatus consisting of the cylindrical swimmer immersed in a circular cylindrical glass tank with radius $R_2 = 10.15$ cm is shown in Fig. 1(a). The swimmer is composed of a polyester sheet with a coating of rubber on the inner surface glued to form an elastic circular cylinder with radius $R_1 = 5.70$ cm. The elastic cylinder is then stretched between two vertical rollers as shown in Fig. 1(a), resulting in a swimmer with a cross section as shown in

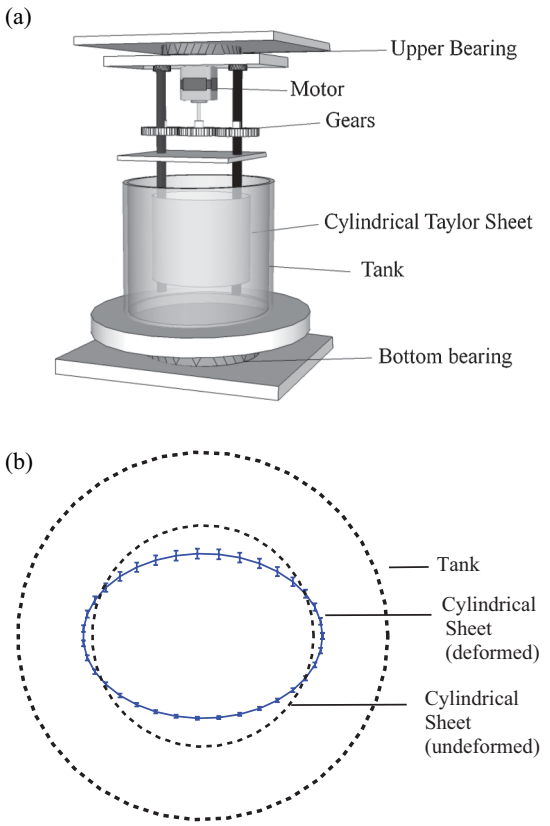

FIG. 1. (Color online) (a) Schematic diagram of the cylindrical swimmer apparatus. (b) The measured shape of the swimmer and error bars as it rotates over several cycles. The undeformed circular sheet with $R_1 = 5.70$ cm and the boundary of the tank with radius $R_2 = 10.15$ cm are also plotted for reference.

Fig. 1(b). An elliptical cross section can be calculated to result using elastic theory if a circular sheet is stretched by applying constant forces along diametrically opposite ends. This shape is observed to describe the measured cross section, which has major semiaxis 6.8 cm and minor semiaxis 4.6 cm. Some deviations are also observed caused by seams and other imperfections in the fabrication of the cylinder. These deviations lead to a maximum of 2.4% deviation in the horizontal direction and 2.8% deviation in the vertical direction from the center as the swimmer rotates. We do not observe deformation of the sheet arising from fluid stresses.

The rollers are then driven with a stepper motor and planetary gear system. This allows the rotation speed of the cylindrical sheet (which equals the phase velocity $\Omega_{\text{sheet}} = 2\pi/T$, where T is the period) to be set and varied over a wide range. Therefore if one follows a point on the surface of the sheet, it moves in and away from the center of the cylinder as it rotates, giving rise to a traveling wave in the azimuthal direction. The tank is placed on a bearing to impose torque-free boundary conditions on the swimmer provided the bearing is frictionless. The frictional coefficient of the bearing is obtained by measuring the decay of the angular speed of the tank set into motion with an initial speed. The friction is found to be small and constant over the range used in our experiments and approximately equal to 0.005 ± 0.0001 N m. The entire swimmer along with gears and motors is mounted on a second rotary bearing from the ceiling to reduce the torques during the initial transient.

Once a traveling wave is imposed on the inner cylinder, the outer cylinder (the tank) starts to rotate in the same direction to minimize torque. In the final steady state the tank rotates with net torque close to zero. Note that the forces exerted by the gears and motors on the oscillating sheet are internal forces, and maintaining torque-free boundary conditions at steady state on the tank ensures that the swimming sheet itself is torque-free. The rotation speed of the tank Ω_{tank} is measured by imaging a marker on the tank. The corresponding swimming speed of the Taylor swimmer is then obtained by

$$\Omega_{\text{swim}} = \Omega_{\text{sheet}} - \Omega_{\text{tank}}. \tag{10}$$

IV. MEASUREMENT OF SWIMMING SPEEDS

A. Newtonian fluids

We first discuss the results with Newtonian fluids in order to provide a reference to compare with swimming in viscoelastic fluids. The properties of the fluids used are noted in Table I. A plot of measured angular speed of the tank Ω_{tank} versus the phase velocity Ω_{sheet} is plotted in Fig. 2(a) for the various liquids. The Reynolds number Re varies between 0.15 and 1.47 for the viscous corn syrup, and between 0.29 and 2.21 for the light corn syrup. We observe that the speeds in the higher-viscosity fluids collapse onto a single line with an intercept close to the origin. The fact that the data can be described by a line is important validation that we are in the linear regime in the experiments. The small intercept with the horizontal axis shown in Fig. 2(a) arises because the viscous drag of the fluid on the boundary is not sufficient at very low frequencies to overcome the friction in the bearing on

TABLE I. List of fluids used in the experiments and their properties. The shear rate viscosities of the viscoelastic fluids are shown in Fig. 4.

Label	Fluid	Kind	η (Pa s)
Viscous CS	Viscous corn syrup	Newtonian	27
Light CS	Light corn syrup	Newtonian	7
Glycerine	Glycerine	Newtonian	0.5
Boger	PAA and corn syrup	Viscoelastic	37
CMC 2%	Carboxymethyl cellulose 2%	Viscoelastic	Shear thinning
CMC 3%	Carboxymethyl cellulose 3%	Viscoelastic	Shear thinning
Polyox 1%	Polyethylene oxide 1%	Viscoelastic	Shear thinning
Polyox 2%	Polyethylene oxide 2%	Viscoelastic	Shear thinning

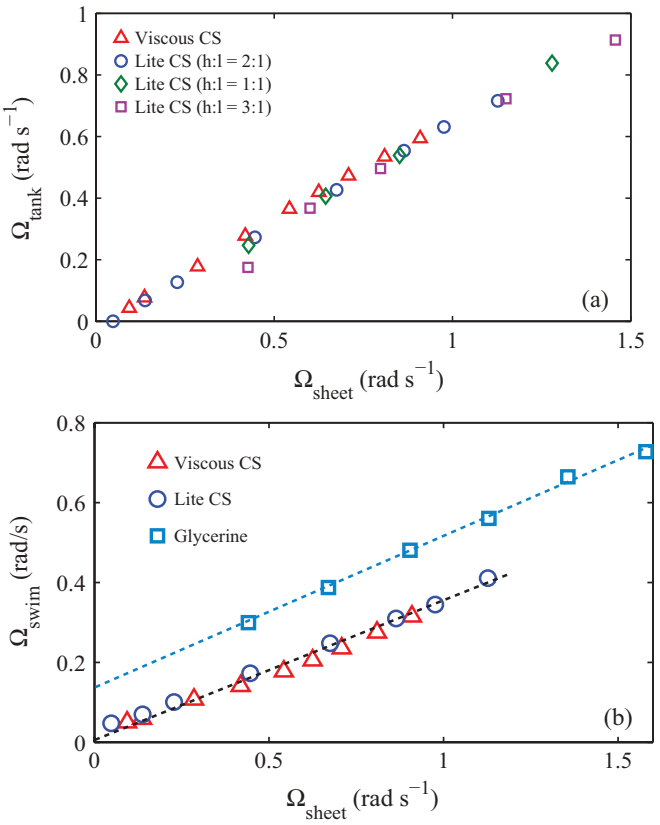

FIG. 2. (Color online) (a) The angular speed of the tank Ω_{tank} versus rotation speed of the inner cylinder Ω_{sheet}. The data correspond to light corn syrup, high-fructose corn syrup, and various ratios of height h of the fluid in the tank to the average gap $R_2 - R_1$. The data are observed to fall on a line with an intercept close to the origin. (b) The angular swimming speed of the Taylor swimmer versus phase velocity in a viscous fluid is described by a linear fit. The friction in the bearing leads to a vertical offset in measured Ω_{swim} for glycerin, which has lower viscosity, but the linear fit has the same slope.

which the tank rotates. Also plotted in Fig. 2(a) are the speeds corresponding to various heights of the viscous liquids in the tank. The measured angular speed collapses onto the same line in all cases. This collapse indicates that the measured speeds are independent of the height of the sheet immersed in the fluid and the top and the bottom surfaces of the tank do not influence the measurements. We further tested the two-dimensional nature of the fluid flow by using a horizontal light sheet using a laser to visualize the flow of small tracer particles. The tracer particles remained on the cross section of the fluid illuminated by the laser, further indicating the two-dimensionality of the system.

As can be noted from Eq. (6), the swimming speed increases linearly with Ω_{sheet} with the slope given by the geometric factor g_f. When the experimentally measured swimming speed Ω_{swim} is then calculated using Eq. (10), and plotted in Fig. 2(b), it is observed to increase linearly with Ω_{sheet} consistent with Eq. (6). The data for viscous corn syrup and light corn syrup collapse onto the same line. However, while the line passes close to the origin, a small intercept with the vertical axis can be noted due to the systematic effect of the friction of the bearing. We have further investigated this effect by using glycerin, which has relatively lower viscosity and thus a greater Ω_{tank} has to be applied to overcome the friction of the bearing. We can note that measured Ω_{swim} for glycerin can be described by a line with same slope as for the higher-viscosity fluids but with a higher vertical intercept. Thus, we find that provided the viscosity of the fluid is large enough, the systematic error introduced by the friction of the bearing is small. Henceforth, we discuss swimming speeds for fluids where the effect of the friction of the bearing on the swimming speed can be considered negligible.

We compare the measured speeds with those obtained using calculations using the Stokes equation in terms of the geometric factor g_f in Eq. (6). The linear fit to the experimental data yields $g_f(\text{expt}) = 0.32$. Approximating the shape of the swimmer with Eq. (1), we calculate $g_f = 0.36$ from Eq. (7). Equation (7) is valid for small deformations given by Eq. (1) from a circular shape, while the actual belt has large deformations and is close to an ellipse. Therefore using COMSOL, we calculated the swimming speed for an ellipse with dimensions matching the belt; in this case $g_f = 0.29$. Furthermore, as noted in the discussion of Fig. 1(b), asymmetries are present in the experimental apparatus. To explore the effect of these asymmetries in our numerical simulations, we offset the center of the swimmer by 2.5% of R_2, and find using COMSOL g_f in the range 0.29 to 0.31, which is close to the experimentally measured value. We conclude that the apparatus shows the main features of an ideal Taylor swimmer including linear dependence on the imposed phase velocity.

B. Viscoelastic fluids

We now discuss the swimming speed of the Taylor swimmer in various fluids which have been typically used to study viscoelasticity. A list of the fluids used can be found Table I. These include two samples of a Boger fluid prepared by mixing 125 ppm polyacrylamide (PAA) in 96.5% viscous corn syrup to obtain a fluid with constant viscosity as a function of shear rate. We also use more complex fluids such as aqueous solutions of carboxymethyl cellulose and polyethylene oxide, which are representative of biological fluids that are often shear thinning. Sodium CMC was mixed 2% and 3% by weight to prepare fluids that we label CMC 2% and CMC 3%, respectively. Polyethylene oxide, commonly known as Polyox, is a water-soluble polymer; it was mixed 1% and 2% by weight in water. We find that the Reynolds number for the viscoelastic fluids used in our experiments varies from 0.05 to 2 for the liquids in our experiments, a range that is similar to the range for Newtonian liquids.

The measured angular swimming velocity as a function of phase velocity is shown in Fig. 3. We observe that the swimming speeds are systematically *faster* in the Boger fluid compared to the Newtonian fluid for the same phase velocity. Thus, the trend observed appears to be qualitatively different from that found for Olroyd-B fluids in Eq. (8) where swimming speeds are always lower than that for the Newtonian fluid. On the other hand, the swimming speed in viscoelastic fluids which mimic shear thinning and have multiple relaxation time constants is found to be systematically *lower* than in the case of the Newtonian fluid for the same phase velocity.

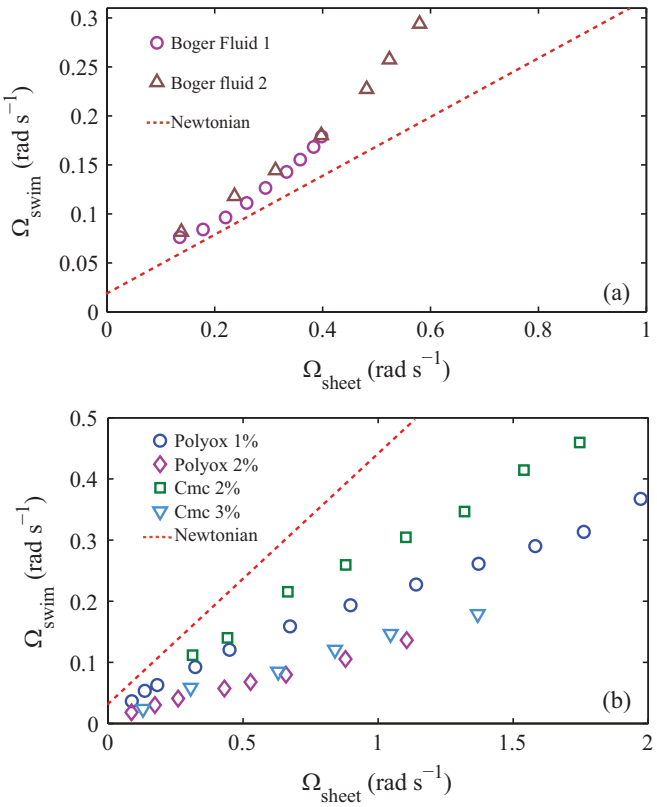

FIG. 3. (Color online) (a) Swimming speed as a function of phase velocity for Boger fluid in comparison to that of Newtonian corn syrup. Systematically greater swimming speeds are observed in the Boger fluid. (b) Swimming speed as a function of phase velocity for Newtonian and viscoelastic fluids. Systematically lower speeds are observed with prescribed angular frequency.

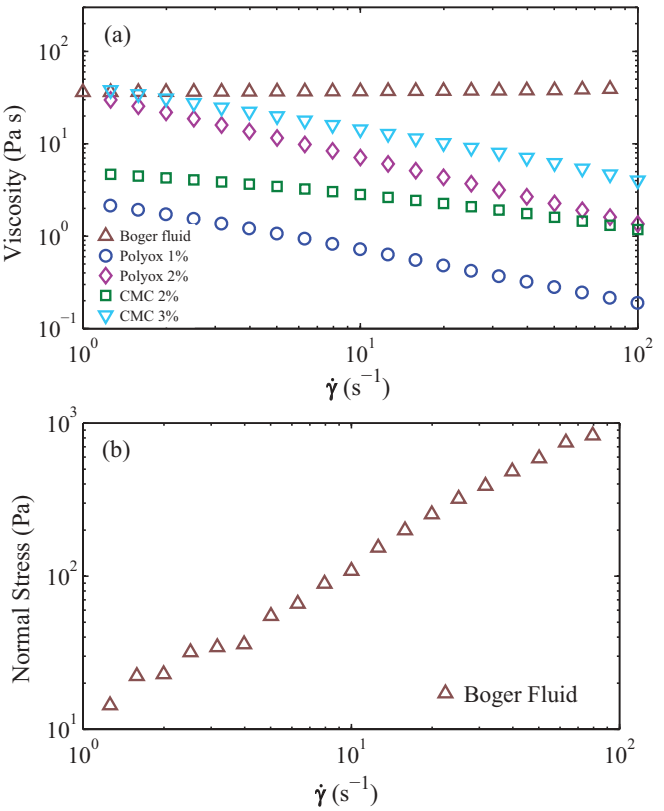

FIG. 4. (Color online) (a) Viscosity as a function of shear rate in Boger fluid, CMC 2%, CMC 3%, Polyox 1%, and Polyox 2%. (b) Normal stress (N) as a function of shear rate in Boger fluid.

C. Rheology

To make a more quantitative comparison between our experiments and the predictions of theory, we measure the rheology of the fluids with a TA Instruments AR 2000 rheometer. The shear-dependence of the fluids is characterized by constant shear-rate measurements. Figure 4(a) shows the shear viscosities of the fluids over a wide range of shear rates $\dot{\gamma}$, from 10^0 to 10^2 s^{-1}. The Boger fluid here (PAA solution) has a shear-rate-independent viscosity $\eta = 37.2 \pm 0.2$ Pa s. The fluid also exhibits elasticity. The normal stress N is observed to increase with shear rate $\dot{\gamma}$ [see Fig. 4(b)]. The viscoelasticity can thus be characterized by the first normal stress coefficient $\Psi = N/\dot{\gamma}^2$ in the limit of vanishing $\dot{\gamma}$ [11]. Due to the lack of experimental accuracy at shear rates below 1 s^{-1}, we cannot access the regime where Ψ depends quadratically on $\dot{\gamma}$. Nevertheless, if we use the values measured at the low end of our experimental regime where we can still obtain the normal stress value with robustness, we find $\Psi = 18.43$ Pa s^2. Based on the viscosity of the Newtonian solvent (96.5% viscous corn syrup), $\eta_s = 26.9 \pm 0.5$ Pa s, we can estimate the longest relaxation time as $\tau = \Psi/[2(\eta - \eta_s)] = 0.9$ s.

In the cases of CMC and Polyox, the viscosities not only increase with polymer concentration but also decrease with shear rate, as shown in Fig. 4(a). Such a shear-thinning feature suggests that these polymeric solutions are not dilute and can no longer be characterized by single relaxation times, as applied to the previous Boger fluids. In this nondilute region, these polymer suspensions are likely to develop shear-rate-dependent networks, which are composed of multiple relaxation modes. To characterize such relaxation modes, we also perform standard linear rheology measurements with small oscillatory shear-strain perturbations [12]. The associated shear moduli are shown in Fig. 5 for a range of oscillation frequency ω that covers our experimental settings. Here, the storage modulus G' gives the component of the response of the stress that is in phase with the oscillatory strain and is associated with the solidlike properties of the material. On the other hand, G'' is the loss modulus, which governs the component of the response of the stress which is in phase with the strain-rate, and is associated with fluidlike properties of the material. Using rheology models including polymer networks [13,14], we can potentially estimate the mean relaxation time $\tau(\omega)$, associated with few effective relaxation modes at given frequency ω. *In situ*, we find that such relaxation times are not too different from those obtained from a much simpler "Maxwell's model" approach, as described in the following.

According to Maxwell's model for a polymeric liquid with a single relaxation time, the moduli G' and G'' can be expressed in terms of the oscillation frequency ω as

$$G' = \frac{\eta\tau\omega^2}{(1+\omega^2\tau^2)} \tag{11}$$

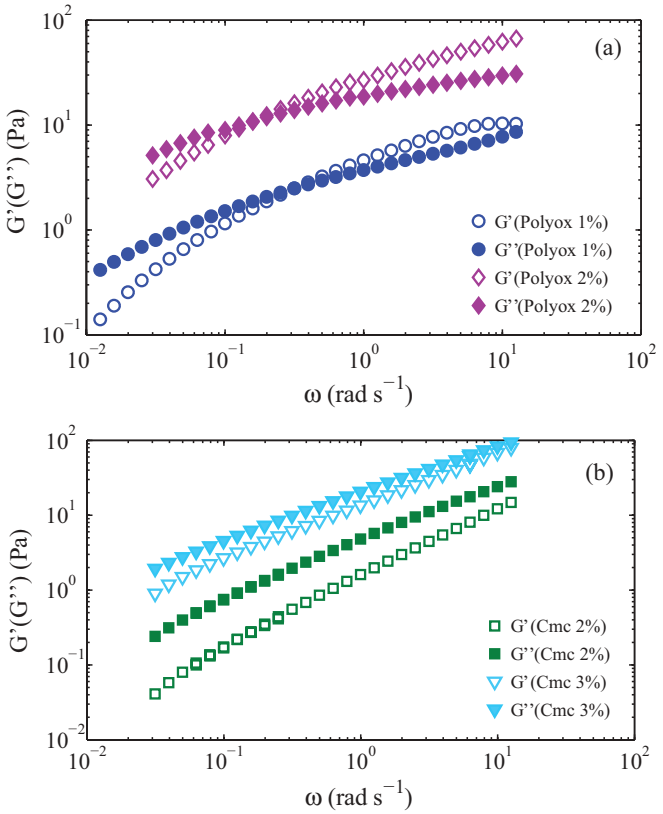

FIG. 5. (Color online) Rheological properties of the fluids used: (a) Polyox and (b) CMC.

and

$$G'' = \frac{\eta\omega}{(1+\omega^2\tau^2)}, \tag{12}$$

where η is the zero-frequency viscosity, and τ is the relaxation time. Therefore, we can calculate the relaxation time as

$$\tau = \frac{G'}{G''\omega}, \tag{13}$$

provided the liquid has a clear single relaxation time scale. If there are multiple modes of relaxation, then G' and G'' are sums of terms as above but with η and τ replaced by $\eta(k)$ and $\tau(k)$, where k runs over the different modes [11]. Because of a lack of a simple scaling in the plots of G' and G'' (shown in Fig. 5) it is difficult to perform an analysis to extract relaxation time constants for these fluids.

To have an estimate of the relaxation time scale, we obtain the relaxation time scale τ from Eq. (13) for that particular driving frequency. This estimate is also reminiscent of the fact that only a few modes of relaxation are efficient at a given oscillation frequency, which can be potentially explained by more sophisticated models including shear-thinning features [13,14]. Thus we can calculate the Deborah number De for the range of angular frequencies and relaxation times spanned in the experiment using Eq. (9). However, in the case of shear-thinning fluids it is not possible to determine the effective relaxation time scale using the same method. In order to have an estimate of the relaxation time scale, we obtain the relaxation time scale τ from Eq. (13) for that particular driving frequency. A similar method was adopted by Shen and Arratia

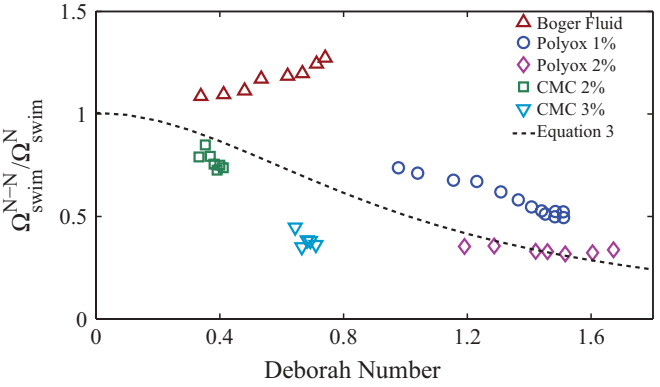

FIG. 6. (Color online) Ratio of non-Newtonian and Newtonian swimming speeds versus the Deborah number. The theoretical prediction for the ratio is plotted as $1/(1+\mathrm{De}^2)$. In interpreting this graph it must be noted that the Boger fluid has a clearly defined relaxation time and therefore De, but De is not well defined in the cases of Polyox and CMC as discussed in the text.

in their report [9] with CMC and therefore we present it here in order to draw comparison with previous work. However, it is important to note that because G' and G'' do not scale according to the Maxwell model with a single relaxation constant it is difficult to justify this method in such fluids.

The ratio of swimming velocities of non-Newtonian and Newtonian fluids is plotted as a function of the Deborah number in Fig. 6. We observe that the ratio of the speeds increases with De for the Boger fluid, but decreases for CMC and Polyox. Thus the behavior partitions along the lines of the shear-thinning properties of the fluid. Given this divergent behavior it is difficult to even conclude that the overall decrease in swimming speeds observed with CMC and Polyox is even qualitatively consistent with calculations performed with Olroyd-B fluids. Note that, although the fluids are shear thinning in nature over a large range of shear rate, the experimental regime of frequencies happens to be small, and hence the viscosity of these fluids in that regime does not seem to vary too much. Also, the fact that the experiments are performed in a low-Reynolds-number regime minimizes the chances of viscosity affecting the swimming speed.

It is further interesting to note that the divergent trends observed in our experiments are consistent with the two other reports with the two kinds of fluids used in our experiments. Liu *et al.* [8] found enhanced swimming speeds with a Boger fluid in a rotating helical geometry, and Shen and Arratia [9] found decreasing swimming speed for the case of live *C. elegans* swimming in CMC. It is possible that the overall behavior is governed by nontrivial interactions between viscous and elastic components that determine swimming speed.

V. CONCLUSIONS

In conclusion, we have designed an apparatus to measure the speed of a swimmer with a prescribed shape as a function of phase velocity. The simplicity of our apparatus makes it an attractive system for measuring swimming speed in non-Newtonian fluids and making comparisons with the predictions of theory. For the Newtonian fluids, the measured speeds are

found to be in agreement with calculations using the Stokes equation. However, the measured speeds in the Boger fluid are in sharp contrast with the form calculated for the Oldroyd-B model of viscoelastic fluids. Interestingly, the swimming speeds in more complex viscoelastic fluids are observed to decrease with concentration and with phase velocity. While this trend is qualitatively similar to the trend calculated for Oldroyd-B fluids, the rheology of *real* non-Newtonian fluids makes it difficult to form a well-defined Deborah number, and hence prevents us from drawing quantitative conclusions about these fluids. Furthermore, although we do not see inertial effects in our Newtonian fluids, we have not ruled them out in our experiments with the non-Newtonian fluids. Our results, which show both increasing and decreasing trends in the same apparatus with the various viscoelastic fluids, point to a pressing need for a broad series of experiments, theory, and numerical simulations in systems with varieties of geometries before we can fully understand how microorganisms swim in viscoelastic fluids.

ACKNOWLEDGMENTS

We thank Fouad Abdulameer for help with experiments. This work was supported by National Science Foundation Grants No. CBET-0853942 (Clark) and No. CBET-854108 (Brown). A.K. and T.R.P. thank the Aspen Center for Physics, which is supported by the National Science Foundation Grant No. PHY-1066293. T.R.P. is grateful to Roman Stocker and the Environmental Microfluidics Group at MIT for hospitality while some of this work was completed.

[1] L. Fauci and R. Dillon, Annu. Rev. Fluid Mech. **38**, 371 (2006).
[2] G. Taylor, Proc. R. Soc. London, A **209**, 447 (1951).
[3] E. Lauga, Phys. Fluids **19**, 083104 (2007).
[4] H. C. Fu, T. R. Powers, and C. W. Wolgemuth, Phys. Rev. Lett. **99**, 258101 (2007).
[5] S. S. Suarez and X. Dai, Biol. Reprod. **46**, 686 (1992).
[6] J. P. Celli, B. S. Turner, N. H. Afdhal, R. H. Ewoldt, G. H. McKinley, R. Bansil, and S. Erramilli, Biomacromolecules **8**, 1580 (2007).
[7] J. Teran, L. Fauci, and M. Shelley, Phys. Rev. Lett. **104**, 038101 (2010).
[8] B. Liu, T. R. Powers, and K. S. Breuer, Proc. Natl. Acad. Sci. USA **108**, 19516 (2011).
[9] X. N. Shen and P. E. Arratia, Phys. Rev. Lett. **106**, 208101 (2011).
[10] A. E. Hosoi and L. Mahadevan, Phys. Rev. Lett. **93**, 137802 (2004).
[11] R. B. Bird, R. C. Armstrong, and O. Hassager, *Dynamics of Polymeric Liquids: Fluid Mechanics*, 2nd ed. (Wiley, New York, 1987).
[12] M. Baumgaertel and H. H. Winter, Rheol. Acta **28**, 511 (1989).
[13] *Proceedings of the IVth International Congress on Rheology, Providence, RI*, edited by H. Giesekus and E. H. Lee, Vol. 15 (Interscience, New York, NY, 1965) Part 3.
[14] D. Acierno, F. P. La Mantia, G. Marrucci, and G. Titomanlio, J. Non-Newton. Fluid Mech. **1**, 125 (1976).